New structural transformations in congruent ferroelectric $LiNbO_3$ fibres evidenced by Raman spectroscopy

2000 J. Phys.: Condens. Matter 12 2305

(http://iopscience.iop.org/0953-8984/12/10/315)

J. Phys.: Condens. Matter **12** (2000) 2305–2316. Printed in the UK PII: S0953-8984(00)07921-2

New structural transformations in congruent ferroelectric $LiNbO_3$ fibres evidenced by Raman spectroscopy

I Noiret†‖, J Lefebvre†, J Schamps‡, F Delattre‡, A Brenier§ and M Ferriol§

† Laboratoire de Dynamique et Structure des Matériaux Moléculaires, UPRESA 8024, UFR de Physique, Bâtiment P5, Université de Lille 1, 59655 Villeneuve d'Ascq Cédex, France
‡ Laboratoire de Physique des Lasers, Atomes et Molécules, UMR 8523 du CNRS, Centre d'Etudes et de Recherches Lasers et Applications, UFR de Physique, Bâtiment P5, Université de Lille 1, 59655 Villeneuve d'Ascq Cédex, France
§ Laboratoire de Physico-Chimie des Matériaux Luminescents, UMR 5620 du CNRS, Université Claude Bernard de Lyon 1, 69622 Villeurbanne, France

E-mail: noiret@lip5rx.univ-lille1.fr

Received 17 September 1999

Abstract. Temperature dependent Stokes and anti-Stokes Raman-scattering experiments have been performed to study the ferroelectric phase of congruent $LiNbO_3$ fibres in the external and internal mode regions. Mode splittings and changes in the slope of frequency–temperature plots at 590 and 790 K show the occurrence of two structural transformations at these temperatures. The anisotropy of the correlation time associated with the width of the central component and anomalies observed in previous neutron investigations are related to a migration process of the lithium atoms along the hexagonal axis and along the pseudo-cubic axis of the highly distorted related perovskite structure. The observed transformations are tentatively assigned to long-range correlated rearrangements in the intrinsic defect structure of the crystal.

1. Introduction

The possibility of growing crystalline niobate fibres of high quality that can be used as non-linear matrix hosts for solid state ion lasers has reinforced the interest that has been focused on lithium niobate since its original synthesis in 1965 [1]. The $LiNbO_3$ fibres under study therein were grown in Lyon using the laser heated pedestal growth method. Detailed characterization of the properties of such doped fibres is a prerequisite in order to control and to use them routinely as optically active media. The present work aims at contributing to this objective. It reports and tentatively interprets the observation of structural transformations through temperature dependent Raman scattering studies.

The properties and applications of lithium niobate have been widely studied, resulting in the publication of several thousand papers on this material. The high level of interest in lithium niobate mainly stems from its outstanding electro-optical and non-linear optical properties. Moreover a large negative birefringence allows phase matching in optical-wave parametric-amplifier experiments [1–4]. Our lithium niobate fibres have been grown in the most ordinary composition for this compound, i.e. the congruent composition $Li/Nb = 0.946$. This congruent structure is known to be highly defective with cation vacancies required for reasons of charge compensation [5]. Among numerous papers,

‖ Correspondence to be sent to I Noiret.

0953-8984/00/102305+12$30.00

various investigations on the structure and chemical composition of $LiNbO_3$ revealed that many physical properties, among which are the extraordinary refractive index and the Curie temperature, depend significantly on the intrinsic defect structure [6]. Therefore the method employed for growing the crystal can be suspected to have an influence on its properties.

Lithium niobate is a crystalline insulator which is ferroelectric at room temperature. Its Curie temperature has been determined to be fairly high, about 1400 K [5]. X-ray diffraction studies by Abrahams and Marsh [7, 8] and by Megaw [9] have shown that, below this temperature, the space group of $LiNbO_3$ is $R3c$. The nature of the ferroelectric–paraelectric phase transition has long been a subject of controversy [10–13] but it seems now accepted that it is of the order–disorder type with a minor displacive component [14, 15]. In the high-temperature paraelectric phase the lithium atoms are randomly distributed over two sites on both sides of the oxygen planes and the niobium atoms assume centrosymmetric positions within their NbO_6 octahedra. In the ferroelectric phase, under study here, the lithium cations are locked in sites located on one definite side, leaving the other vacant. At the same time the niobium cations are displaced out of the centres of their oxygen octahedra that become distorted. Along the threefold axis, the structure appears as made of the repetition of the following sequence of three successive octahedra sharing faces and given by order of increasing size: niobium-containing octahedron, lithium-containing octahedron, empty octahedron.

The vast majority of studies on $LiNbO_3$ have been carried out at room temperature. Only a few of them explored the temperature dependence of the properties of the ferroelectric phase that extends up to 1400 K. Among them, some x-ray diffraction and neutron diffuse scattering analyses [14–16] as well as dielectric constant measurements [17] have pointed out several interesting anomalies in the temperature dependence of the dynamic properties of the ferroelectric phase. These anomalies have been sometimes hypothetically assigned to unspecified phase transitions but most often no clear physical explanation has been proposed. In view of this, the major purpose of the present paper was to use another method of investigation to confirm and to ascertain the presence of these anomalies in the case of fibres. This was done via the Raman scattering study of the vibration modes in the temperature range (300–1300) K. Slope breakings and mode splittings have been systematically looked for. Particular attention has been devoted to the central component. Finally an interpretation of the experimental results is tentatively given in terms of ion migration within the intrinsically defective structure of congruent $LiNbO_3$.

2. Experimental procedures

The Raman spectrum of lithium niobate has been studied rather extensively [18–23] but this is the first time that temperature-dependent Raman scattering experiments have been carried out on crystalline fibres grown from a congruent composition (48.8% Li_2O) by the laser heated pedestal growth (LHPG) method [24, 25]. The single-crystal fibres employed had typically a diameter of 0.5 mm and a length of 5 mm. They were colourless and transparent. The use of oriented seeds enabled the growth of crystals along different axes. For this study, they were grown along the $\boldsymbol{c}$ axis. In the experiments this fibre axis was aligned along the laboratory z axis and the a fibre axis is parallel to the incident beam. The experiments were carried out over the fairly extended (300–1300) K temperature range using a compressed-hot-air stream system. Above 1300 K the increase in the absorption at the exciting and scattered radiation frequencies becomes considerable, which makes the resolution very poor. The Raman scattering spectra were recorded at different

temperatures separated by regularly spaced steps of 15 K. The change from one temperature to the next was carried out very slowly, typically in one hour or more, to ensure perfect stabilization. This point was important in order to observe clearly the transformations discussed below.

For the Raman scattering experiments the sample was excited by the light beam of an Ar^+ laser with a constant output of 100 mW at 4880 Å. The scattered light was analysed using a Coderg T800 triple monochromator with an instrumental resolution of 1 cm^{-1}. For each selected temperature the output signal was detected with a photon counter (Princeton Applied Research 1109) and recorded via a Dilor data acquisition system over the -1000 cm^{-1} to $+1000$ cm^{-1} frequency region. The spectra obtained in the right-angle scattering geometry were recorded at high resolution ($\sim$1 cm^{-1}) and with long scanning times in order to have good statistics (typically five hours). Thus, no doubt was left concerning the observation of the lines, even those with the weakest intensities.

The line frequencies were then measured to high accuracy by simultaneously fitting the Stokes and anti-Stokes parts of the spectrum recorded in the same scan using damped oscillator profiles. This procedure eliminates the error that arises from using the exciting line as the reference point to measure the Raman shifts. The central component was analysed on the basis of a relaxator function and the spectra were corrected for the thermal factors.

It is important to note the reproducibility of the Raman spectra for several samples of the same fibre. However very slowly increasing temperature was necessary condition to observe clearly the transformations discussed below. It was unfortunately impossible to perform the study over a complete cycle because the quality of the sample was irreversibly destroyed when a high temperature was reached.

3. Results

3.1. Raman spectra at room temperature

The $LiNbO_3$ lattice can be described either in terms of the rhombohedral or hexagonal systems. The hexagonal conventional cell contains three rhombohedral unit cells. Throughout the present paper the notations for the axes are those of the hexagonal system with the threefold axis as the $\boldsymbol{c}$ axis and the $\boldsymbol{a}$ axis perpendicular to a glide plane. In the ferroelectric phase, lithium niobate has the $R3c$ space group structure with $3m$ point group symmetry. There are two molecules per rhombohedral unit cell and therefore 30 vibrational degrees of freedom. Vibrations with zero wave-vector $\boldsymbol{q}$ may be characterized group theoretically as $5A_1$, $5A_2$ and 10 (doubly degenerate) E phonons. Of these, one A_1 and one E correspond to the three acoustic branches, the five A_2 fundamentals are both Raman and infrared inactive and the remaining four A_1 and nine E optical branches are both Raman and infrared active. Since all of these 13 modes which are Raman active carry polarization, their interaction with the macroscopic field produced by the infrared-active phonons for $\boldsymbol{q} = 0$ gives rise for each one to longitudinal (LO) and transverse (TO) components. The directional dispersion of these extraordinary phonons has been widely studied by Claus *et al* [26] within the context of the backward scattering method.

Figure 1 shows spectra obtained at 300 K for the two different scattering configurations vv and hh corresponding respectively to the (zz) and (xy) Raman tensor elements. After deconvolution of the spectra, 17 distinct modes are observed in both vv and hh scattering geometries. These 17 modes are listed in columns 1 and 2 of table 1 for both polarizations. Some of them have a very weak intensity but they must be included in order to fit satisfactorily the spectra.

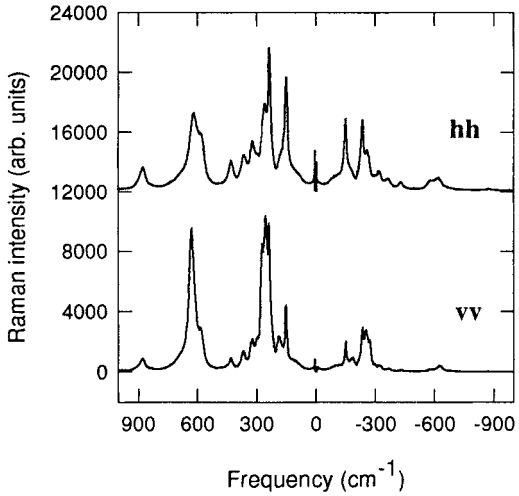

Figure 1. Stokes and anti-Stokes Raman spectra of $LiNbO_3$ in the vv and hh polarization at room temperature.

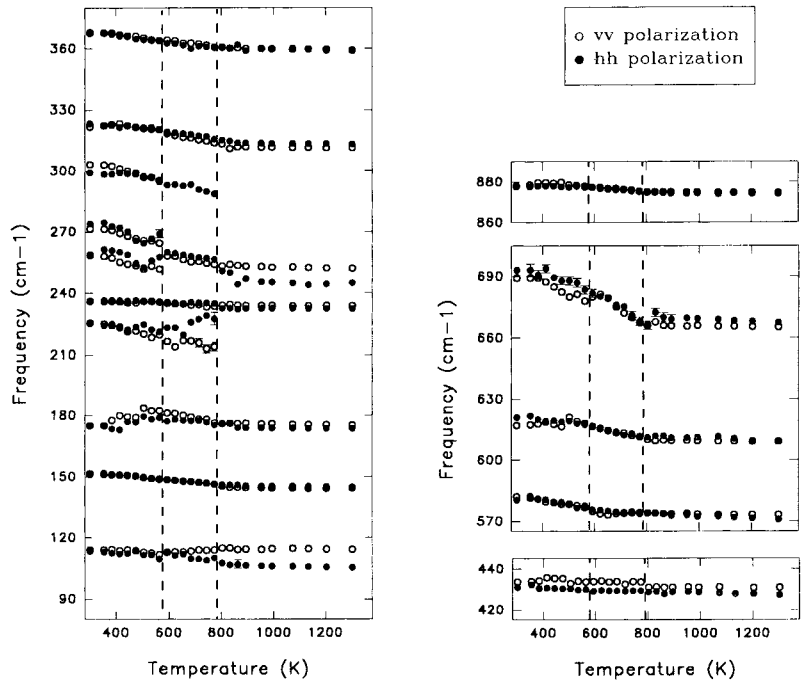

Figure 2. Frequency–temperature dependence of the modes observed in the vv (○) and hh (●) polarizations.

It is noteworthy that the modes observed in the fibre, either in hh or vv polarization, correspond to the majority of the modes recorded by Claus *et al* [26] for the $\theta = 0^\circ$ and $\theta = 90^\circ$ limiting geometries. For instance the two modes observed clearly separated at 580

Table 1. Frequencies of the vibration modes active at room temperature in vv and hh scattering geometries in Raman spectra of $LiNbO_3$. The temperatures above which the modes disappear are indicated between brackets.

Frequency (cm^{-1})			
Noiret *et al*		Claus *et al*	
vv	hh	vv	hh
114	*116*	[a]	[a]
152	**151**		**155** E(T)
185	*180*	*198* E(L)	
225 (790 K)	*225* (790 K)		
237	*236*	*243* E(L)	**238** E(T)
252 (590 K)	*252* (590 K)	**255** A(T)	
261 (590 K)	*261* (590 K)		*265* E(T)
275	*274*	**276** A(T)	*275* A(L)
300 (790 K)	*299* (790 K)	*295* E(L)	
322	**322**		*325* E(T)
332 (590 K)	*332* (590 K)	*333* A(T)	**334** A(L)
369	**368**		**371** E(T)
433	**431**		*431* E(T)
			436 A(L)
581	**580**		**582** E(T)
628	*624*	**633** A(T)	
693	*697*	**668** E(L)	*668* E(T)
			743 E(T)
880	**878**		**876** A(L)

In the fibre of the present work (Noiret *et al*), all the modes were observed both in vv and hh polarization. Types of character give a scale for relative intensities: for a given mode, the polarization for which the frequency is written in bold type is that for which the mode is the most intense; the other is written in light italics.

In the bulk (Claus *et al*) most of the modes appear in only one of the two polarizations. In this case, the bold/light convention refers to comparison of the intensities of modes continuously connected in the directional dispersion pattern between hh and vv polarization (see figure 1 of [26]).

Very faint modes are written in small characters.

[a] Broad peaks observed by Claus *et al* [26] and attributed to difference bands.

and 628 cm^{-1} both in hh and vv polarization in our fibre spectra are the modes Claus *et al* observed for $\theta = 0^\circ$ (E_{TO} mode at 582 cm^{-1}) and $\theta = 90^\circ$ (A_{TO} mode at 633 cm^{-1}) in their bulk spectra; these modes correspond in fact to the extreme values arising from a gradual shift of the frequency when θ varies continuously from 0 to 90° (directional dispersion). We did not observe two modes reported by Claus *et al* as E(TO) modes at 668 and 743 cm^{-1}. These were shown recently not to be due to normal $LiNbO_3$ phonons by Ridah *et al* [27] on the basis of a comparison between Raman scattering spectra of congruent and nearly stoichiometric $LiNbO_3$. It can be noticed that, as expected, the A_{TO} modes are enhanced in vv polarization whereas the E_{TO} modes are enhanced in hh polarization. Thus, taking the example of the 580 cm^{-1} (E_{TO}) and 628 cm^{-1} (A_{TO}) modes, the first one is more intense than the second in hh polarization and vice versa in vv polarization.

The occurrence of such a mode 'leakthrough' could be assigned to the occurrence of strong internal strains as suggested by other authors who found the same phenomenon even in their bulk phase samples [10]. Other reasons could also be put forward to explain the observed

breaking of usual selection rules such as waveguiding effects specific to the fibre, influence of spatial dispersion on light scattering [26] or strong interactions between the modes associated with large anharmonicity of the vibrational movements. Moreover samples of congruently grown lithium niobate must necessarily contain a large number of on-site substitutions and compensating vacancies to ensure charge neutrality [5]. In such highly defective crystals, strict lattice periodicity is removed so that symmetry-forbidden transitions can become significantly allowed.

3.2. Temperature dependence of the phonons

The temperature dependence of the frequencies of the vibrational modes is reported in figure 2. This dependence is strictly the same in both geometries. It reveals unambiguously two new phenomena at about 590 and 790 K.

Below 590 K the spectra contain 17 vibrational modes (those of table 1). The spectra above 590 K can be fitted with only 14 damped oscillators: the 261 and 275 cm^{-1} modes collapse into a single 263 cm^{-1} mode while the 252 and 332 cm^{-1} modes disappear. Moreover, at this temperature of 590 K, slope breakings are observed in the 581, 628 and 693 cm^{-1} high frequency modes. Then, above 790 K, a correct fit of the experimental spectra can be obtained with 12 modes: the modes at 224 and 303 cm^{-1} disappear. Moreover some discontinuities are also observed (see figure 2). The temperature dependences of the widths of the most significant fundamental modes (at 237, 322, 369 and 628 cm^{-1}) are reported in figure 3 and all of them clearly display changes in the slopes at 590 and 790 K. Note that these modes (except for the 236 cm^{-1} one) are isolated enough to prevent the evolution of their widths from being influenced by the splitting or by the disappearance of modes. Thus, for the 322 cm^{-1} mode, the width of this line is constant from room temperature up to 590 K, then it exhibits a linear temperature dependence between 590 and 790 K followed by a slight curvature above 790 K (see figure 3(b)) without any peculiar frequency shift.

3.3. Temperature dependence of the central component

Spectral features typical of weakly disordered and/or defective systems have been observed, namely broad phonon bands (especially at 628 cm^{-1}) and quasi-elastic scattering. With increasing temperature, the quasi-elastic scattering becomes exceedingly broad. This is illustrated in the spectrum of figure 4 recorded at 950 K. At these temperatures, the poor signal-to-noise ratio does not enable us to perform a reliable determination of the changes in phonon dampings and couplings. Accordingly the width of the central component has been associated with a correlation time describing the statistical behaviour of the disorder. This correlation time τ has an exponential temperature dependence: $\tau = \tau_0 \exp[W/kT]$. In this expression the activation energy W is the height of the potential barrier separating the wells. Figure 5 shows the evolution of the inverse of the central component linewidth (τ) versus temperature for both polarizations. The τ_0 and W constants have been estimated by fitting the $\tau(T)$ function to the experimental data between 300 and 1300 K (figure 5).

The heights of the potential barrier energies obtained for both polarizations ($W/k = 580$ K for vv and 1240 K for hh) are rather small, which rules out the hypothesis of an orientational disorder. As discussed in the next section, this is more likely the mark of a diffusion process than of disorder. The fact that the value of W determined from the vv polarization spectrum is almost one half of the value obtained in the hh polarization indicates the existence of a preferential direction of migration along the hexagonal axis.

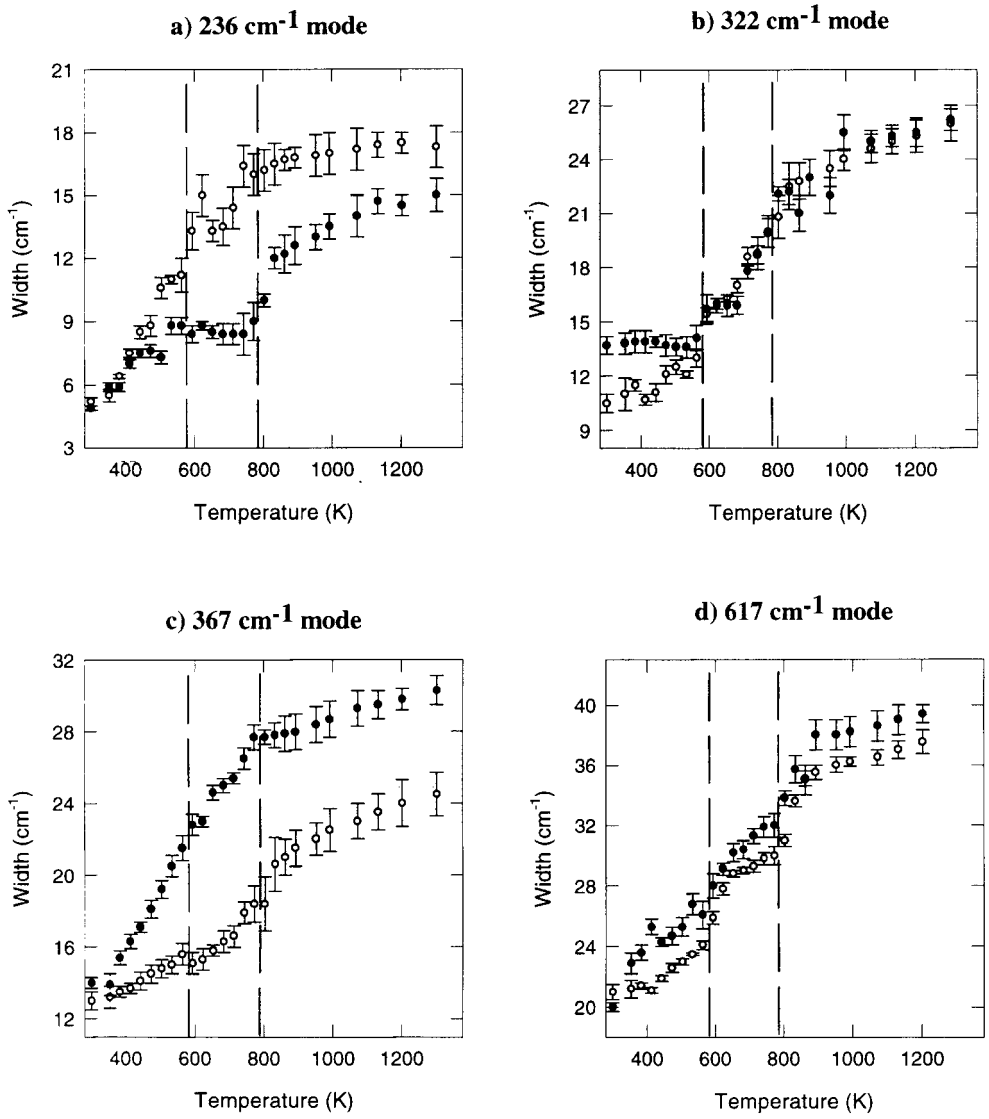

Figure 3. Temperature dependence of the linewidth of (a) the 236 cm^{-1} mode, (b) the 322 cm^{-1} mode, (c) the 367 cm^{-1} mode, (d) the 617 cm^{-1} mode in the vv (○) and hh (●) polarizations.

3.4. Structural transformations due to heating

The unit cell parameters have been determined at room temperature by x-ray diffraction on an Enraf Nonius CAD-4 diffractometer before and after having run the Raman scattering experiments. The results show a large irreversible increase of the unit cell volume after heating at 1300 K: $V_{initial} = 310$ Å^3 and $V_{final} = 317$ Å^3. Moreover photography of the irradiated $LiNbO_3$ fibre by back-reflection Laue x-ray diffraction showed clearly a diffuse circle superimposed on the diffraction pattern. This suggests that, on increasing temperature, the $LiNbO_3$ fibre suffers a deterioration probably rather similar to that found in the Li_3NbO_4

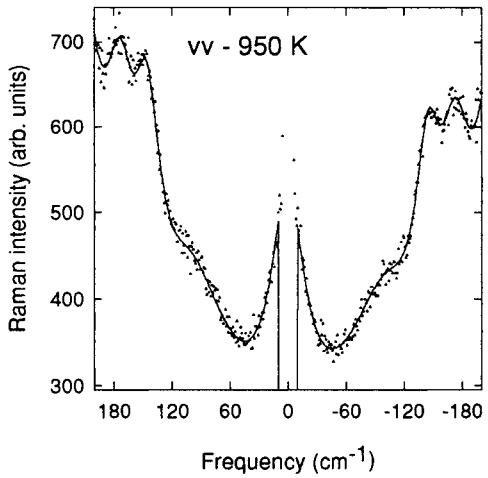

Figure 4. Raman spectrum of $LiNbO_3$ in the vv polarization at 950 K.

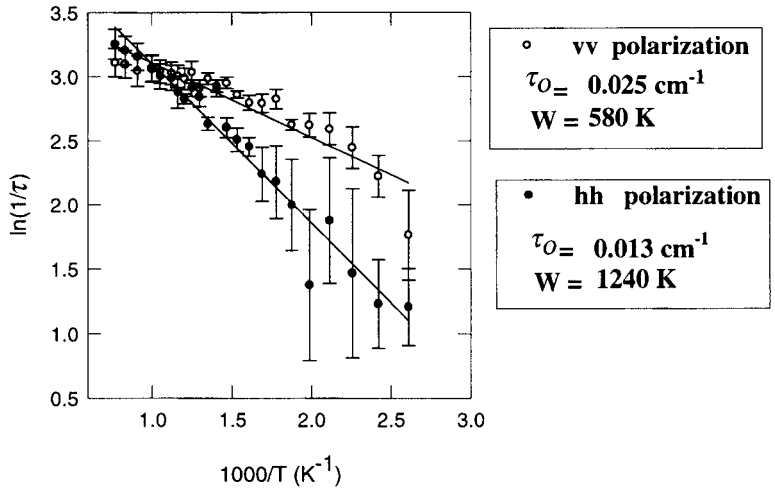

Figure 5. Temperature dependence of the correlation time τ.

crystal [28]. In this compound, x-ray diffraction experiments have shown that the Li:Nb cationic ratio deviates from the 3:1 stoichiometric composition on heating. Li^+ ions tend to gradually disappear thus creating a Li-deficient site. Another reason, specifically linked to the experimental conditions, could be the chemical reactions which take place predominantly at the surface of the sample at high temperature (irreversible oxidation reactions).

4. Discussion

The anomalies that clearly appear at 590 and 790 K in our Raman spectra (see figure 2) have been found in all of the fibre samples we have tested. Related phenomena have also been observed by several authors in $LiNbO_3$ in congruent crystals grown via other methods. Thus, thermal expansion 'anomalies' have been reported in the same range of temperature

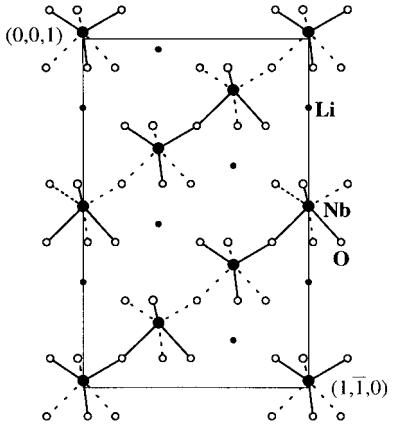

Figure 6. Projection of the $LiNbO_3$ structure. Lithium atoms (small black circles) are represented as individual ions while niobium atoms (large black circles) are linked by full lines (in and over the plane) and dotted lines (behind the plane) to oxygens (open circles) so as to show NbO_6 octahedra. The figure exhibits parallel endless chains of NbO_6 octahedra and lithium ions. These chains are oriented along the pseudo-cubic axis of the related perovskite structure which is oriented at 52° with respect to the *c* axis.

by Ismailzade [16] and Smolenskii *et al* [17]. In the x-ray diffraction experiments carried out by Ismailzade [16] an odd behaviour for both the *a* and *c* parameters has been pointed out: above a range of linear dilatation, it was found that the *c* parameter becomes suddenly almost constant between 773 and 858 K while the *a* parameter keeps on increasing regularly; at 858 K, the temperature evolutions of both parameters undergo a noticeable discontinuity (about 0.01 Å) resulting in a sudden cell volume increase of about 1.5 $Å^3$. Moreover, a differential thermal analysis of the same specimen showed clearly an exothermic effect in this temperature range, confirming that some rearrangement had taken place. Similarly, anharmonic thermal motions above about 600 K have been observed by Ivanov *et al* [29] and an anomaly at 800 K on the integrated intensities of the diffuse scattering has been pointed out recently by Zotov *et al* [15]. Note that these two last temperatures are almost exactly those corresponding to the spectral changes in the Raman scattering spectra reported in figure 2, i.e. 590 and 790 K. These observations and ours undoubtedly reflect different experimental aspects of the same phenomenon. Moreover, the second of these temperatures lies gratifyingly within the range (773–858 K) over which the thermal expansion anomalies have been observed by Ismailzade [16]. This network of compatible experimental facts reveals the occurrence of transformations at about 590 and 790 K within the ferroelectric phase when congruent $LiNbO_3$ is gradually heated.

We suggest in the following an interpretation of these transformations in terms of migration of the lithium ions. Under favourable conditions to be exemplified below, vacant sites may indeed constitute attractive places for neighbouring lithium ions as soon as these can surmount the potential barrier and jump across the distorted oxygen triangles that separate Li-occupied from unoccupied sites. Such migration processes can take place either in the direction of the $\boldsymbol{c}$ hexagonal axis or in directions oriented at about 52° from the hexagonal axis i.e. those directions that correspond to pseudo-cubic axes of the very distorted [30] perovskite structure (see figure 6).

Both types of migration appear to have been observed now. Thus migrations along the hexagonal axis have been suggested above (section 3.2) to explain the observed anisotropy of the relaxation time associated with the central peak component. In this case, a lithium ion can jump into the nearby vacant site under the force due to repulsion from the nearby niobium ion. On the other hand, diffusive motions along a pseudo-cubic axis have been briefly quoted as a plausible interpretation for certain observations arising from neutron investigations on powders [14, 15]. Although the mechanism is the same for both types of migration process, the conditions for their occurrence are somewhat different. Consider first diffusion along the

hexagonal axis. Vacant sites exist naturally along this axis in the ideal perfectly grown $R3c$ structure of $LiNbO_3$ (one vacancy every three sites). In this case, a lithium cation can jump into the nearby vacant site along the c direction under the influence of the repulsive force from the nearby niobium cation. Of course this migration brings the displaced Li^+ ion close to another Nb^{5+} ion so that the inverse process can in turn take place and put back the Li^+ ion in its original location. In some respects, one can view this local oscillation between two sites along c as a dynamic precursor of an order–disorder transition that will lead ultimately to the paraelectric phase above a temperature high enough to generalize the process over the whole crystal.

At this level, diffusion along the hexagonal axis is not likely to correspond to temperature-localized transformations. In order to achieve a preference for one location there must be some disequilibrium. This can be achieved due to some local defect structure, such as that we are going to introduce below for the second type of diffusive motion. On this occasion, it will be shown that a correlation in the defect structure can lead to anomalies called here 'transformations'. Note incidentally that the defect structure is a subsidiary condition for diffusion along the hexagonal axis whereas it will be shown now to be essential to create vacancies for explaining diffusion along the pseudo-cubic axis.

In the ideal $LiNbO_3$ structure all the sites along a pseudo-cubic axis are filled with Li atoms separated by oxygen triangles orthogonal to this axis so that no diffusive motion is allowed along this axis. Any attempt to obtain some insight into the microscopic mechanism that still leads to diffusion must take into account the point defect structure necessarily present in the Li_2O-deficient $LiNbO_3$ imperfect crystal for obvious reasons of charge compensation [5]. Up to now several possible intrinsic defect structure models have been suggested and tested against experiment [31–33] but the choice among them has not yet been brought to a firm conclusion [34]. Even though most recent papers [33, 35, 36] seem to be inclined to favour the so-called Li-deficient model introduced by Lerner *et al* [37], the Nb-deficient model postulated by Abrahams and Marsh [7] cannot yet be definitely ruled out. It may even be possible that both defect structures can be realized depending on the specific growing conditions. In the Li-deficient model, a number of vacancies are created at the Li sites but some of them accommodate 'antisite' Nb atoms. Accounting for charge compensation, the Li-deficient defect structure can be schematically written as $[Li_{1-4x}Nb_x\square_{4x}][Nb]O_3$ (x positive, $\square$ denotes a vacancy).

According to the above elements of interpretation, the remarkable reproducibility of the observed phenomena reveals an underlying organization in the intrinsic defect structure of the congruent $LiNbO_3$ crystal. Without assuming a perfectly periodic organization of the defects over the whole single crystal, it is likely that long-range correlations govern the relative distribution of lithium vacancies and antisite Nb_{Li}^{5+} substitutions along the pseudo-cubic axis. From this point of view it is more convenient to consider the phenomena observed at 590 and 790 K (and maybe others, less easy to identify) as transformations of the intrinsic defect structure considered as a locally organized sub-structure within the framework of the mean $R3c$ ferroelectric ideal lattice of $LiNbO_3$. To be more concrete, consider as an example among many others the following defective sequence of cations in a chain of lithium sites along the pseudo-cubic axis with one antisite niobium and one vacancy located as follows:

$$\ldots Li^+(1)Nb_{Li}^{5+}Li^+(2)Li^+(3)\square Li^+(4)\ldots.$$

The potential wells that accommodate those cationic sites are separated by steric barriers corresponding to the energy required to cross distorted oxygen triangles of comparable (but significantly different) sizes. The effect of defects in the parallel chains can be disregarded in a first approximation on account of the purely qualitative nature of the discussion. The highly charged antisite Nb_{Li}^{5+} ion repels strongly the nearby lithium ions. Those ions on the left-hand

side (like $Li^+(1)$) are locked by their like neighbours but, for high enough temperature, the $Li^+(2)$ and $Li^+(3)$ ions have the opportunity of lowering the electrostatic energy by diffusing towards the vacancy on their right-hand side. The process takes place in two steps: first $Li^+(3)$ migrates into the vacancy then $Li^+(2)$ jumps into the new vacancy arising from the $Li^+(3)$ migration. The same phenomenon is expected to occur at the same (or nearly the same) temperature for every local arrangement identical (or nearly identical) to the one described here. A large number of similar diffusion processes involving the cooperative association of both antisite niobium ions and vacancies but with different cationic stacking arrangements could also be described. Each of them corresponds to another 'defect transition' temperature. From the macroscopic experimental point of view, this gives the phenomenon the appearance of a diffuse transformation that extends over a wide range of temperature. But at the microscopic level this diffuse transformation actually corresponds to an infinite set of transition points in the frustrated intrinsic defect structure.

As a matter of fact, the full quantitative interpretation of these complex processes of intrinsic defect structure reorganization under the influence of temperature remains a real challenge for further theoretical studies. Nevertheless the above interpretation is sufficient to provide a key for understanding and for unifying, at least at a qualitative level, a number of puzzling experimental data. According to this interpretation, it appears that the intrinsic defect structure of congruent $LiNbO_3$ acts as an underlying structure that possesses its own kinetics and organization subject to the overlying $R3c$ structure of the crystal.

Acknowledgments

The authors are much indebted to G Boulon, M T Cohen-Adad and G Foulon for their participation in growing the crystals and for helpful discussions. The Centre d'Etudes et Recherche Lasers et Applications (CERLA) is supported by the Ministère chargé de la Recherche, the région Nord/Pas de Calais and the Fonds Européens de Développement Economique des Régions.

References

[1] Ballman A A 1965 *J. Am. Ceram. Soc.* **48** 112
[2] Fedolov A, Shapiro Z I and Ladyzhinskii P B 1965 *Sov. Phys.–Crystallogr.* **10** 218
[3] Boyd G D, Miller R C, Nassau K, Bond W L and Savage A 1964 *Appl. Phys. Lett.* **5** 234
[4] Giordmaine J A and Miller R C 1965 *Phys. Rev. Lett.* **14** 973
[5] Schirmer O F, Thiemann O and Wöhlecke M 1991 *J. Phys. Chem. Solids* **52** 185
[6] Bergman J G, Ashkin A, Ballman A A, Dziedzic J M, Levinstein H J and Smith R G 1968 *Appl. Phys. Lett.* **12** 92
[7] Abrahams S C and Marsh P 1986 *Acta Crystallogr.* B **42** 61
[8] Abrahams S C 1994 *Acta Crystallogr.* A **50** 658
[9] Megaw H D 1968 *Acta Crystallogr.* A **24** 583
[10] Johnston W D and Kaminow I P 1968 *Phys. Rev.* **168** 1045
[11] Penna A F, Porto S P S and Chaves A S 1976 *Solid State Commun.* **19** 491
[12] Chaudhury M R, Peckham G E and Saundarson D H 1978 *J. Phys. C: Solid State Phys.* **11** 1971
[13] Mendes-Filho J, Lemos V and Cerdeira F 1984 *J. Raman Spectrosc.* **15** 367
[14] Boysen H and Altorfer F 1994 *Acta Crystallogr.* B **50** 405
[15] Zotov N, Frey F, Boysen H, Lehnert H, Hornsteiner A, Strauss B, Sonntag R, Mayer H M, Güthoff F and Hohlwein D 1995 *Acta Crystallogr.* B **51** 961
[16] Ismailzade I G 1965 *Sov. Phys.–Crystallogr.* **10** 235
[17] Smolenskii G A, Krainik N N, Khuchua N P, Zhdanova V V and Mylnikova I E 1966 *Phys. Status Solidi* **13** 309
[18] Voron'ko Yu K, Kudryavtsev B A, Osiko V V, Sobol' A A and Sorokin E V 1987 *Sov. Phys.–Solid State* **29** 771
[19] Kojima S 1994 *Ferroelectrics* **152** 301

[20] Barker A S and Loudon R 1967 *Phys. Rev.* **158** 433
[21] Sidorov N V and Serebryakov Yu A 1994 *Vib. Spectrosc.* **6** 215
[22] Andonov P, Chieux P and Kimura S 1993 *J. Phys.: Condens. Matter* **5** 4865
[23] Yang X, Lan G, Li B and Wang H 1987 *Phys. Status Solidi* b **141** 287
[24] Feigelson R S 1986 *J. Cryst. Growth* **79** 669
[25] Foulon G, Ferriol M, Brenier A, Cohen-Adad M T and Boulon G 1995 *Chem. Phys. Lett.* **245** 555
[26] Claus R, Borstel G, Wiesendanger E and Steffan L 1972 *Z. Naturf.* a **27** 1187
[27] Ridah A, Bourson P, Fontana M D and Malovichko G 1997 *J. Phys.: Condens. Matter* **9** 9687
[28] Shishido T, Suzuki H, Ukei K, Hibiya T and Fukuda T 1996 *J. Alloys Compounds* **234** 256
[29] Ivanov S A, Choney S A, Mikhal'chenko V P and Venevtsev Yu N 1979 *Ukr. Phys. J.* **24** 662
[30] Megaw H D and Darlington C N W 1975 *Acta Crystallogr.* A **31** 161
[31] Bollmann W 1983 *Cryst. Res. Technol.* **18** 1147
[32] Suzuki T 1996 *J. Cryst. Growth* **163** 403
[33] Watanabe Y, Sota T, Suzuki K, Iyi N, Kitamura K and Kimura S 1995 *J. Phys.: Condens. Matter* **7** 3627
[34] Donnerberg H J, Tomlinson S M and Catlow C R A 1991 *J. Phys. Chem. Solids* **52** 201
[35] Iyi N, Kitamura K, Izumi F, Yamamoto J K, Hayashi T, Asano H and Kimura S 1992 *J. Solid State Chem.* **101** 340
[36] Wilkinson A P, Cheetham A K and Garman R H 1993 *J. Appl. Phys.* **74** 3080
[37] Lerner P, Legras C and Dumas J P 1968 *J. Cryst. Growth* **3/4** 231